Flows of particle-laden Bingham fluids in a Hele-Shaw cell

S. Boronin[1], A. Osiptsov[1] & J. Desroches[2]
[1]*Schlumberger Moscow Research, Moscow, Russian Federation*
[2]*Services Petroliers Schlumberger, Paris La Defense Cedex, France*

Abstract

We consider the multiphase flow of immiscible particle-laden Bingham fluids in a Hele-Shaw cell. The flow is described within the framework of interpenetrating-continua model with account for particle velocity slip. Using lubrication approximation, a system of governing equations is reduced to a quasilinear equation in terms of pressure and transport equations for volume concentrations of fluids and particles. The numerical solution is obtained on a rectangular mesh using a finite-difference method. The pressure equation is solved using an iterative algorithm and preconditioned Bi-Conjugated Gradient-Stabilized method, while transport equations are solved using a second-order TVD flux-limiting scheme with the Superbee limiter. The model and numerical algorithm are validated against experiments on particle-free gravitational slumping and viscous fingering, as well as against experiments of particle-laden suspension flow with sediment layer growth. In particular, particle transport and settling are validated against experimental data and an analytical formula for the height of a packed bed. Numerical simulations show that the slumping rate of Bingham fluid is significantly less pronounced than that of a Newtonian fluid with the same density and viscosity. If a low viscosity fluid is injected after the Bingham one, the Saffman-Taylor instability at the interface leads to the development of fingers and origination of unyielded zones.
Keywords: Bingham rheology, viscous fingering, gravitational slumping, particles, Hele-Shaw cell.

WIT Transactions on Engineering Sciences, Vol 79,
www.witpress.com, ISSN 1743-3533 (on-line)
doi:10.2495/MPF130121

1 Introduction

With the expansion and development of industrial processes and technologies including hydraulic fracturing and cleanup of hydraulically fractured wells, modeling of non-Newtonian fluid flows in naturally fractured reservoirs [1] and hydraulic fractures [2] is becoming important. A theoretical analysis of such flows is usually complicated and requires the formulation of mathematical models accounting for various physical phenomena including development of waves and instability at fluid-fluid interfaces, fluid slumping, particle transport and settling, granular packing and fluid leak-off through porous walls into surrounding rock formation.

A large number of papers deal with plane-parallel flows of Bingham fluids between rigid boundaries (see review of analytical solutions for the velocity profile of Bingham fluid flows in simple geometries [3] and more recent studies [4, 5]). Only a few studies in the open literature are devoted to two-dimensional flows of Bingham fluids. In [6, 7], the authors analyze the interaction of Bingham fluids in a circular annulus in application to primary cementing of an oil well. Study [8] deals with the instability of the front between Bingham fluids in a Hele-Shaw cell within the framework of linear approach. It is found that the instability condition is similar to those for Newtonian fluids, but involves yield stresses. In the case considered, the fastest growing disturbances at the interface between two fluids are those with the smallest wavelength, as there is no cut-off mechanism, which exists in case of non-zero surface tension, where the fastest growing disturbances have some finite wave length. Even at very small injection velocity a large amplification is gained by small-wavelength disturbances. Small fingers left behind in the beginning of the destabilization tend to stop.

To the best of our knowledge, a comprehensive analysis of interactions of Bingham particle-laden fluids in a narrow slot has not been carried out yet. The aim of the present study is to analyze various physical phenomena accompanying multiphase flow in a Hele-Shaw cell, such as combined effect of gravitational slumping and viscous fingering, particle settling and granular packing.

2 Two-continua model

We consider a flow of a mixture of non-Newtonian particle-laden fluids in a fracture, which is modeled as a Hele-Shaw cell. The suspension flow is described within the framework of the two-continuum approach [9–11], where the two interpenetrating continua are assumed to be a carrier medium (fluid), and a dispersed continuum (particles). Particles are assumed to be large enough to omit their Brownian motion, and their diameter is much smaller than the length scale of the flow. Carrier fluid is composed of several immiscible fluids. We do not track the interface between the fluids, instead we describe the fluid distribution in the slot by tracers, limited to three in this study, C_0, C_1, C_2 ($C_0+C_1+C_2 = 1$), each of which representing the concentration of a single carrier fluid. We also assume that there will be a narrow mixing zone in the vicinity of interfaces. This assumption is justified in the limit of low fluid miscibility and

small surface tension, which is relevant for the applications targeted by this paper. We introduce a Cartesian coordinate system with the origin at the middle-plane of the slot and Oxy plane parallel to the walls (axis *y* is vertical). The full system of 3D governing equations reads like:

$$\frac{\partial\left(1-C_p\right)C_i}{\partial t}+\mathrm{div}\left[\left(1-C_p\right)C_i\mathbf{v}_f\right]=0,\ i=0,1,2;\ \frac{\partial C_p}{\partial t}+\mathrm{div}\left[C_p\mathbf{v}_p\right]=0 \tag{1}$$

$$\rho_f\frac{\mathrm{d}_f\mathbf{v}_f}{\mathrm{d}t}=-\nabla p_f+\nabla_j\tau_f^{ij}\mathbf{e}_i+\rho_f\mathbf{g}-n_pF_p,\ \rho_p\frac{\mathrm{d}_p\mathbf{v}_p}{\mathrm{d}t}=-\nabla p_p+\nabla_j\tau_p^{ij}\mathbf{e}_i+\rho_p\mathbf{g}+n_pF_p \tag{2}$$

Here, subscripts '*f*' and '*p*' denote parameters of the fluids and particles, p_f and p_p are pressures in the carrier fluid and the dispersed phase; τ_f^{ij} and τ_p^{ij} are viscous-stress tensors of the phases, n_p is the number concentration of particles, F_p is the force acting on a single particle; $\mathrm{d}_f/\mathrm{d}t$ and $\mathrm{d}_p/\mathrm{d}t$ are corresponding material derivatives. Averaged densities of the phases are determined as follows:

$$\rho_i=\left(1-C_p\right)C_i\rho_i^0,\ i=0,1,2;\ \rho_p=C_p\rho_p^0 \tag{3}$$

where ρ_i^0 and ρ_p^0 are the substance densities of *i*-th fluid and the particles.

We assume that the particle-laden suspension is described by the Bingham rheology. The stress tensor in the particulate phase can be neglected in the continuum mechanics sense, based on assumption that particles do not oscillate, so that their momentum is transferred with mass-averaged velocity only. The stress tensor of the particle-laden suspension is as follows:

$$p_m^{ij}=-p_f\delta^{ij}+\tau_m^{ij},\quad \tau_m^{ij}=\tau_m^{ij}(e^{ij}),e^{ij}=\frac{1}{2}\left(\nabla^j v_f^i+\nabla^i v_f^j\right) \tag{4}$$

$$\begin{cases}\tau_m^{ij}=2\left(\mu_m+\tau_m\left|\dot{\gamma}\right|^{-1}\right)\left(e^{ij}-\dfrac{1}{3}div\,\mathbf{v}_f\right),\ \tau>\tau_m,\ \tau=\sqrt{\dfrac{1}{2}\tau_{ls}\tau^{ls}},\ \dot{\gamma}=\sqrt{2e_{ls}e^{ls}}\\ e^{ij}=0,\quad \tau<\tau_m\end{cases} \tag{5}$$

Here, μ_m (C_i, C_p) is the plastic viscosity and τ_m(C_i, C_p) is the yield stress of the mixture, τ is the second invariant of the viscous stress tensor of the suspension τ_m^{ij}, and $\dot{\gamma}$ is the shear rate (doubled second invariant of the strain-rate tensor e_{ij}).

The force acting on a single spherical particle moving in an unsteady shear flow at low Reynolds number (based on the particle velocity slip) comprises several components in addition to the Stokes drag [12]. In the conditions typical of oilfield applications, the interphase momentum exchange can described by the Stokes drag and the buoyancy force:

$$F_p=6\pi\sigma\mu_0\left(\mathbf{v}_f-\mathbf{v}_p\right)-\frac{4}{3}\pi\sigma^3\rho_f^*\mathbf{g},\ \rho_f^*=C_0\rho_0^0+C_1\rho_1^0+C_2\rho_2^0 \tag{6}$$

Here, ρ_f^* is the density of the carrier fluid substance (density of the carrier fluid in the absence of particles).

We choose to determine the viscosity of the suspension by Scott's formula [13]:

$$\mu_m\left(C_0,C_1,C_2,C_p\right)=\mu_m^0\left(C_0,C_1,C_2\right)\left(1-\frac{C_p}{C_{\max}}\right)^{-1.89},$$

where μ_m^0 is the viscosity of the particle-free mixture of fluids, $C_{\max}$ is the maximum packing concentration.

The boundary conditions for the system of governing equations (1)–(2), are as follows:

$$x=0:\mathbf{v}_f=\mathbf{v}_{f0}(t,y,z),\mathbf{v}_p=\mathbf{v}_{p0}(t,y,z),C=C(t,y,z) \tag{7}$$

$$z=\pm\frac{w(t,x,y)}{2}:u_f=v_f=0,w_f=\pm\frac{1}{2}\frac{\partial w}{\partial t}\pm v_l,w_p=0 \tag{8}$$

here, w is the half-width of the slot, v_l is the leak-off velocity in case of porous walls.

We introduce the non-dimensional variables as follows (the dimensional variables are denoted by a prime, when required to distinguish them from the dimensionless ones):

$$x'=Lx,\ y'=Ly,\ z'=Lz,\ \mathbf{v}_f'=U\mathbf{v}_f,\ \mathbf{v}_p'=U\mathbf{v}_p,\ t'=\frac{L}{U}t,\ \rho_i'=\rho_0^0\rho_i \tag{9}$$

$$\rho_p'=\rho_0^0\rho_p,\ (\tau^{ij})'=\frac{\mu_0 U}{L}\tau^{ij},\ p'=\frac{\rho_0^0U^2}{\mathrm{Re}}p,\ \nabla'=\frac{1}{L}\nabla,\ \zeta=\frac{\rho_p^0}{\rho_0^0},\ w'=Lw \tag{10}$$

$$v_l'=Uv_l,\ \mathrm{Re}=\frac{\rho_1^0Ud}{\mu_0},\ \mathrm{Bu}_0=\frac{\mathrm{Re}}{\varepsilon^2\mathrm{Fr}^2}=\frac{\rho_1^0gL^2}{\mu_0U},\ \varepsilon=\frac{d}{L} \tag{11}$$

Here, L and U are slot length and velocity scaling factors, d is the slot width, ρ_0^0 and μ_0 are substance density and plateau viscosity of the fluid '0', Re is the Reynolds number and Bu_0 is the Buoyancy number based on the slot length L.
The non-dimensional densities of the carrier fluid, the dispersed phase, and the mixture are as follows:

$$\rho_f=\left(1-C_p\right)\left(C_0+C_1\zeta_1+C_2\zeta_2\right),\quad \rho_p=C_p\zeta_p,\quad \rho_m=\rho_f+\rho_p \tag{12}$$

The momentum conservation equations for the mixture and particles in the non-dimensional form are written as follows:

$$\varepsilon^{-1}\mathrm{Re}\left[\rho_f\frac{d\mathbf{v}_f}{dt}+\rho_p\frac{d_p\mathbf{v}_p}{dt}\right]=-\nabla p_f+\nabla_j\tau_m^{ij}\mathbf{e}_i-\mathrm{Bu}_0\rho_m\mathbf{e}_2 \tag{13}$$

$$\varepsilon\mathrm{St}\frac{d_p\mathbf{v}_p}{dt}=\mu\left(C_p\right)\left(\mathbf{v}_f-\mathbf{v}_p\right)-\frac{\mathrm{St}}{\mathrm{Fr}^2}\left(1-\frac{C_0+C_1\zeta_1+C_2\zeta_2}{\zeta_p}\right)\mathbf{e}_2 \tag{14}$$

$$\begin{cases}\tau_m^{ij}=2\left(\mu_m+\mathrm{Bn}\,\tau_m\left|\dot{\gamma}\right|^{-1}\right)\left(e^{ij}-\dfrac{1}{3}div\,\mathbf{v}_f\right),\ \tau>\mathrm{Bn}\,\tau_m\\ e^{ij}=0,\quad \tau<\mathrm{Bn}\,\tau_m\end{cases}$$

The independent governing dimensionless parameters involved in the non-dimensional system of governing equations are:

$$\varepsilon = \frac{d}{L}, \mathrm{St} = \frac{mU}{6\pi\sigma\mu_0 d}, \mathrm{Fr} = \frac{U}{\sqrt{gd}}, \mathrm{Re} = \frac{\rho_f^0 U d}{\mu}, \zeta_1 = \frac{\rho_1^0}{\rho_0^0}, \zeta_2 = \frac{\rho_2^0}{\rho_0^0} \tag{15}$$

$$\zeta_p = \frac{\rho_p^0}{\rho_0^0}, \mathrm{Bn} = \frac{\tau_0 d}{U\mu_0}, k_1 = \frac{\mu_1}{\mu_0}, k_2 = \frac{\mu_2}{\mu_0}, \kappa_1 = \frac{\tau_1}{\tau_0}, \kappa_1 = \frac{\tau_2}{\tau_0} \tag{16}$$

Here, μ_i and τ_i are viscosities and yield stresses of the fluids.

3 Lubrication approximation

We consider the asymptotic limit of Eqs. (1), (13)–(14), which corresponds to the suspension flow in a narrow fracture with the width varying slowly at the large length scale:

$$\varepsilon << 1, \ \nabla w << 1, \ \mathrm{St} \sim 1, \ \mathrm{Fr} \sim 1, \ \mathrm{Re} \sim 1, \ \zeta_i \sim 1, \ k_i \sim 1 \tag{17}$$

The following stretched variables are introduced:

$$z = \varepsilon z_1, w = \varepsilon w_1, v_l = \varepsilon v_{l1}, w_f = \varepsilon w_{f1}, p = \varepsilon^{-2} p_1 \tag{18}$$

The other variables are assumed to be of order unity.

Substituting relations (17), (18) into Eq. (13) and neglecting all terms of order ε and smaller, we obtain the following equations:

$$\frac{\partial p_f}{\partial x} = \frac{\partial \tau_{13}}{\partial z}, \frac{\partial p_f}{\partial y} + \mathrm{Bu}\rho_m = \frac{\partial \tau_{23}}{\partial z}, \frac{\partial p_f}{\partial z} = 0, \mathrm{Bu} = \frac{\mathrm{Re}}{\mathrm{Fr}^2} = \frac{\rho_0^0 g d^2}{\mu_0 U} \tag{19}$$

Equations (19) are solved using the no-slip condition on the walls at $z = \pm w/2$ as follows:

$$u_f = \frac{w^2}{8\mu_m}\frac{\partial p}{\partial x}\left(\left[\frac{z}{w/2}\right]^2 - 1 - \frac{4\mathrm{Bn}\,\tau_m}{w\left|\nabla p_f\right|}\left[\frac{|z|}{w/2} - 1\right]\right) \tag{20}$$

$$v_f = \frac{w^2}{8\mu_m}\left(\frac{\partial p}{\partial y} + \mathrm{Bu}\rho_m\right)\left(\left[\frac{z}{w/2}\right]^2 - 1 - \frac{4\mathrm{Bn}\,\tau_m}{w\left|\nabla p_f\right|}\left[\frac{|z|}{w/2} - 1\right]\right) \tag{21}$$

Note that the expressions for velocity components (20)–(21) are nonlinear with respect to the pressure p_f in contrast to the case of Newtonian fluid flow (Bn = 0), where the non-linear terms are absent.

The expression for particle velocity slip can be obtained from Eq. (14), which in the limit of $\varepsilon \to 0$ is turned into the following expression:

$$\mathbf{v}_s = \mathbf{v}_p - \mathbf{v}_f = -\frac{\mathrm{St}}{\mathrm{Fr}^2}\left(1 - \frac{C_0 + C_1\zeta_1 + C_2\zeta_2}{\eta_p}\right) f(C_p)\mathbf{e}_2, \ f(C_p) = \left(1 - \frac{C_p}{C_{\max}}\right)^{\alpha} \tag{22}$$

Exponent α in the expression (22) is a free parameter and it should be determined according to the experimental data; in the simulations we use $\alpha = 5$ similar to [13, 14].

We now apply the cross-slot averaging procedure to governing equations (1), (13)–(14) and the system of governing equations is reduced to the following equations [11]:

$$\frac{\partial w(1-C_p)C_i}{\partial t} + \mathrm{div}\left(w\left[1-C_p\right]C_i\tilde{\mathbf{v}}_f\right) = -2v_l(1-C_p)C_i, \quad i = 1,2 \tag{23}$$

$$\frac{\partial wC_p}{\partial t} + \mathrm{div}\left(wC_p\left[\tilde{\mathbf{v}}_f + \tilde{\mathbf{v}}_s\right]\right) = 0_l, \ \mathrm{div}\left(\frac{w^3}{12\mu_m}g(\varphi)\nabla p - wC_p\mathbf{v}_s\right) = -\frac{\partial w}{\partial t} - 2v_l \tag{24}$$

$$\tilde{\mathbf{v}}_f = -\frac{w^2}{12\mu_m}G(\varphi)\nabla p, \ G(\varphi) = 1 - 3\varphi + 4\varphi^3, \ \varphi = \frac{\mathrm{Bn}\,\tau_m}{w\left|\nabla p_f\right|}$$

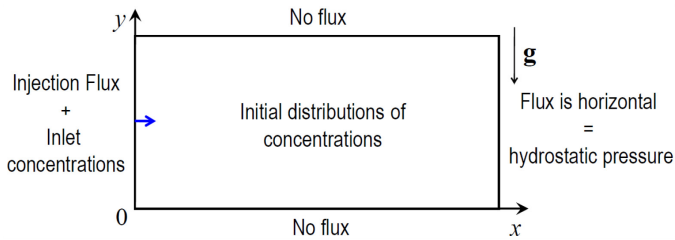

Figure 1: Schematics of boundary and initial conditions.

Note that in Eqs. (23)–(24) differential operators div(·) and ∇ act in (x, y) plane.

Width-averaged governing equations are subject to initial and boundary conditions shown in Fig. 1. As the equations (23) and (24) are hyperbolic, we specify initial distribution of the tracers $C_i(x,y,0)$ and the particle concentration $C_p(x,y,0)$, as well as the concentrations at the inlet $C_i(0,y,t)$, $C_p(0,y,t)$. There is no flux through horizontal boundaries, specified injection flux at the inlet, and condition of zero vertical velocity at the outlet. In order to solve the elliptic equation for pressure (second in Eq. (24)), we reformulate these boundary conditions (7)–(8) to either conditions of first or second kind at all boundaries of the flow domain (i.e., pressure derivatives in the normal direction to all the boundaries, except for the outlet where we prescribe hydrostatic pressure distribution calculated as an integral over the height with account for a possibly non-uniform density distribution).

4 Notes on the numerical solution

The system of Eqs. (23)–(24) is solved numerically using the finite-difference approach. We introduce staggered uniform rectangular mesh with step $h_x = L/N$ in horizontal and $h_y = H/M$ in vertical direction (H is the slot height), $\Delta t_i > 0$ is the time step. The discretization of governing equations is carried out using the standard 5-point "star" stencil.

Numerical solution is obtained using a semi-implicit approach, which allows us to split the solution of equations for pressure and advection (similar to IMPES scheme for fluid flows in porous media). At each time step, the equation for pressure (24) is solved using an iterative algorithm. The non-linear correction to fluid mobility $G(\varphi)$ (see Eq. (24)) is calculated using pressure distribution at the previous iteration (or at the previous time step, if it is the first iteration). Regularization for Bingham viscosity is introduced, so that the mobility of Bingham fluid G is positive everywhere in the flow domain (it is required to avoid degeneration of linear system for pressure). The coefficients and free terms, which depend on the fluid or particle concentrations, are calculated using the distributions at the previous time step. The resulting linear system for pressure is solved using Bi-Conjugated Gradient-Stabilized algorithm with $ILU(2)$ preconditioner [15]. We choose as convergence criterion the norm of difference between pressure fields (relative to the total pressure norm) obtained at the current and previous iterations becoming smaller than a pre-defined small value. The next step involves the calculation of velocity fields for fluids and particles followed by the solution of advection equations by a second-order TVD flux-limiting scheme [16], where the time step is specified according to the CFL condition.

5 Validation of the model and the numerical algorithm

The model and numerical algorithm are validated against the experiment on gravitational slumping of heavy oil in a slot. Initially, left half of the slot is occupied by oil and the right half by air. One of the intermediate positions of oil-air interface observed in the experiment is shown in Fig. 2 by the white line (photo). Dimensions of the slot are 0.15m×0.1m (L×H). Non-dimensional parameters (15)–(16) are as follows: $\mathrm{Bu} = 4\cdot10^{-2}$, $\zeta = 9.35\cdot10^{-4}$, $k = 3.1\cdot10^{-2}$, $\varepsilon = 10^{-2}$ (Fluid 0 is oil, Fluid 1 is air). The numerical simulations of oil slumping in a slot are carried out using 225×150 mesh, (Fig. 2, gray line, same time instant after the start of slumping as in the photo). The evolution of the oil front is well described by the simulations; the discrepancy is mainly due to no-slip of oil at boundaries of the slot, which is not taken into account by the model.

The development of viscous fingers due to Saffman-Taylor instability at the interface between two viscous fluids is validated against the experimental data

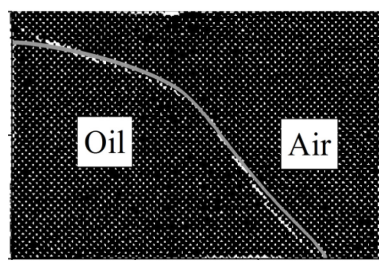

Figure 2: Oil-air interface in the slot.

reported in [17] (Fig. 3). Water-glycerine solution (with a viscosity 84, 9 and 3 times larger than that of the water) is displaced by dyed water in a slot with dimensions 0.2m×0.1m (L×H). Experiments were carried out in microgravity conditions (during a parabolic flight of Airbus A300 Zero-G), and therefore, the effect of gravity was almost eliminated.

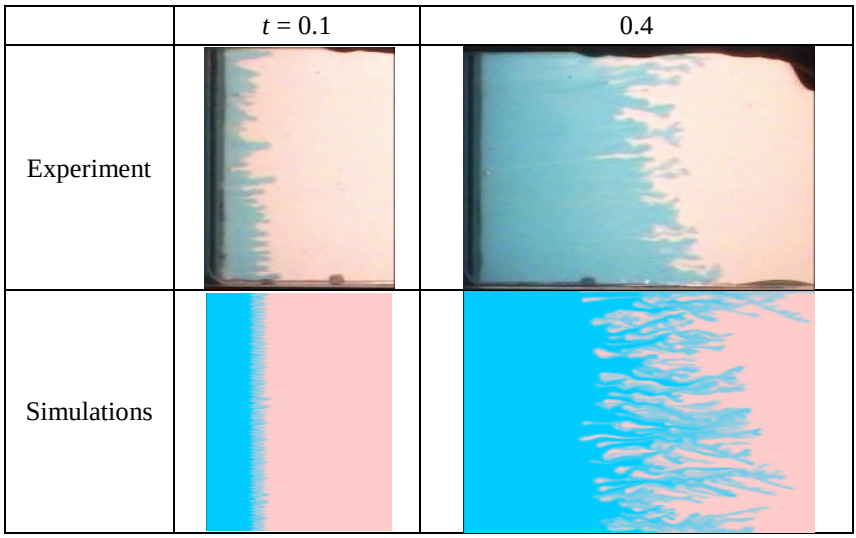

Figure 3: Fingering in a slot [17] (top plots) against the numerical simulations for different time instants (dimensionless).

It is found that the patterns of fingers observed in the experiment and obtained numerically are similar in the case of the viscosity ratio of 9, although the penetration length is overestimated. Simulations of injection carried out at different viscosity ratios (84 and 3) showed an increase in the penetration length with an increase in the viscosity ratio, which is in agreement with the experimental data [17].

The shape of the fingers is affected by the surface tension (or diffusion) significantly, as these mechanisms damp small wavelength instability [1]. In the multiphase model (23)–(24) the finger width is determined by the numerical diffusion at the interface induced by the finite-difference scheme. We believe that for applications it is rather important to predict penetration length of fingers and height-averaged concentration profiles, while the finger patterns are excessively detailed information. Numerical simulations of viscous fingering carried out using different meshes showed that height-averaged profiles (and thus the penetration length) of the invading fluid depend on mesh resolution only slightly. A comparison of height-averaged tracer concentration profiles with the experimental data shown in Fig. 3, t = 0.4, is presented in Fig. 4 (left plot). The width of the mixing zone obtained numerically is slightly larger than that seen in experiment.

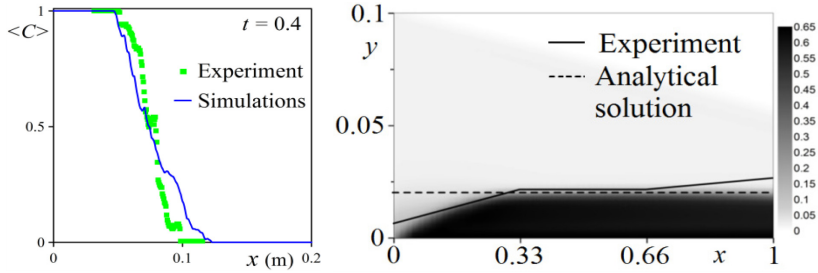

Figure 4: Height-averaged fluid tracer concentration along a slot (left) and distribution of particles in a slot (right).

The approach outlined in this paper was also used to run simulations of particle-laden suspension flow in a rectangular slot. The single fluid carrying particles is Newtonian. The values of the non-dimensional parameters (15)–(16) specified in the simulations are as follows: the slot width-to-length ratio $\varepsilon = 3.3 \cdot 10^{-3}$, height-to-length ratio is 0.1, the inlet concentration $C_p = 0.02$, the maximum packing concentration $C_{\max} = 0.65$, the exponent in the expression for settling velocity $\alpha = 5$, the buoyancy number $\mathrm{Bu} = 848$, the particle-to-fluid density ratio $\zeta_p = 2.6$, and the other parameters are irrelevant for this case, dimensionless time is $t = 26$.

Such flow can develop a packed bed of particles at the bottom of the slot. An analytical solution of the packed-bed height at final equilibrium is given by:

$$H = t \frac{2a^2(\rho_p - \rho_f)g}{9\mu_0} \frac{C_p}{C_{\max}} \left(1 - \frac{C_p}{C_{\max}}\right)^{\alpha-1} \tag{25}$$

Here H is height, t is time since the start of injection, C_p is the inlet particle volume fraction, and α is an exponent in the expression for particle settling velocity (22). This analytical result considers a 1D approximation for the flow under the assumptions that the interface is flat and the concentration just above the interface is equal to the inlet concentration.

Figure 4 (right plot) compares the analytical solution (25) with the distribution of particles obtained in the simulation and in the experiment. There is good agreement between those results, the analytical formula for the height of packed bed on the bottom of a slot and the experimental data, validating the approach described above.

6 Results and discussion

Using the approach outlined above, simulations are carried out to study particle-free fluid-fluid interaction in a slot in the presence of both gravitational slumping and numerical diffusion (no particles). We consider a rectangular slot with aspect ratio 1:1, width-to-length ratio $\varepsilon = 8.6 \cdot 10^{-5}$. Several injection sequences are considered. Each sequence comprises a train of fluids, each characterized by its rheology and density, and a particular volume of each of these fluids. The aim of

these simulations is to study the effect of the sequence characteristics on fingering. For each sequence, three fluids are considered: Fluid 0 is Bingham, while Fluids 1 and 2 are Newtonian. The values of the non-dimensional parameters (15)-(16) specified in the simulations are as follows: Bu = 12.9, Bn = 1.48, $k_1 = 8.72 \cdot 10^{-4}$, $k_2 = 1.43$, $\zeta_1 = \zeta_2 = 0.5$, $\tau_1 = \tau_2 = 0$.

The details of the first sequence that was considered are as follows (dimensionless time intervals of the sequences are shown in parenthesis): Fluid 2 (initially) – Fluid 0 (0.064) – Fluid 2 (0.026) – Fluid 1 (0.043) – No injection (0.21). The results at the end of the sequence are shown in Figs. 4–5 (dimensionless time instants are shown in the right top corner of plots, Fluid 0 is black, Fluid 1 is white and Fluid 2 is gray). In the absence of fingers, when the Bingham fluid occupies the full height of the slot, the behavior is similar to that of a Newtonian fluid: the Bingham correction to fluid mobility is small (which corresponds to a narrow unyielded zone across the slot, see right column of plots in Fig. 5). In the presence of fingers of low-viscosity fluid, however, the advection of Bingham fluid slows down, local pressure gradients decrease and Fluid 0 becomes essentially unyielded (see the right bottom plot in Fig. 5). Simulations are carried out to study the effect of yield stress (determined by the Bingham number Bn). It is found that an increase in Bn leads to a decrease in slumping rate of Bingham fluid and increase in finger penetration length.

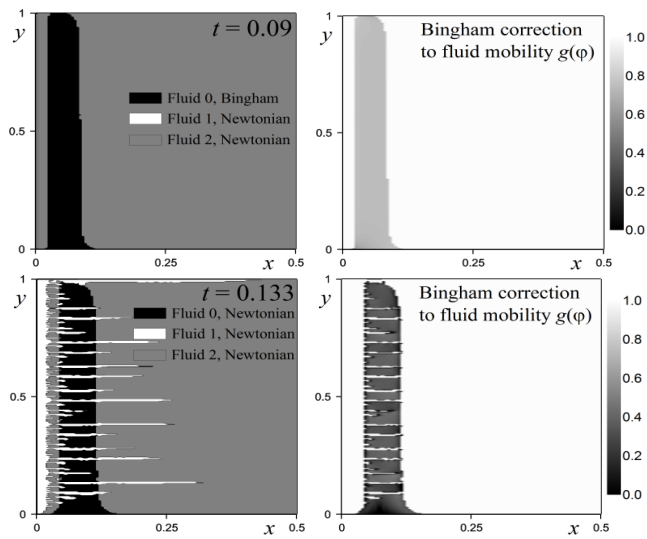

Figure 5: Distribution of fluids at $t = 0.09$ (top) and $t = 0.133$ (bottom).

The left plot in Fig. 6 shows the distribution of fluids with Bingham rheology of Fluid 0 after the stop of injection ($\Delta t = 0.21$), while at the right plot we show the distribution of fluids after the similar injection sequence, but with Newtonian Fluid 0 (same viscosity and zero yield stress). As expected, slumping rate of Bingham fluid is significantly lower than that of Newtonian one.

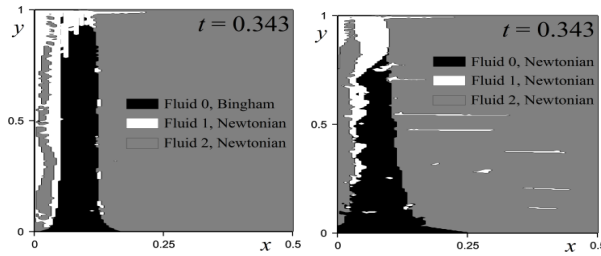

Figure 6: Fluid distribution at $t = 0.343$, black fluid is Bingham (left) and Newtonian (right).

7 Conclusions

A model for particle-laden multiphase flow in a Hele-Shaw cell is formulated within the framework of two-continuum approach. In the limit of a narrow slot, the system of width-averaged equations is derived, which involves the transport equations for concentration of fluids and particles, as well as an elliptic equation in terms of pressure. The numerical solution is obtained using finite-difference method and staggered rectangular grid. The non-linear equation for pressure is solved using an iterative algorithm. At each iteration, the solution of a linear system is carried out using a preconditioned Bi-Conjugated Gradient-Stabilized method. Transport equations are solved using TVD flux-limiting scheme. The simulations are run to first validate the approach using experiments of slumping fluids, fingering and particle transport in a slot. After validation, simulations are conducted to study the effect of Bingham rheology on the development of fingers in a Hele-Shaw cell. It is found that in the presence of fingers at the interface between Bingham and Newtonian fluids, the former becomes essentially unyielded. A finite yield stress leads to significant decrease in fluid mobility compared to the case of Newtonian rheology, which is found to mitigate gravitational slumping. This study could be further extended by comparison of the model predictions with actual lab data for non-Newtonian fluid-fluid displacements. The model of particle transport could be developed further to take into account the solid mechanics effects of particle jamming and transition to close packing.

Acknowledgements

The authors are grateful to A. Ortega for the image processing of fingering experiments and to B. Theuveny and M. Miller for the support of this work.

References

[1] D. Biryukov, F.J. Kuchuk, Transient Pressure Behavior of Reservoirs with Discrete Conductive Faults and Fractures, Transport in Porous Media, Vol. 95, Issue 1, pp. 239-268 (2012).

[2] C.E. Cohen et al., Optimum Fluid and Proppant Selection for Hydraulic Fracturing in Shale Gas Reservoirs: a Parametric Study Based on

Fracturing-to-Production Simulations, SPE paper N 163876-MS, 2013 SPE Hydraulic Fracturing Technology Conference, Feb 04-06, 2013, The Woodlands, USA.
[3] R.B. Bird, G.C. Dai and B.J. Yarusso, J. The rheology and flow of viscoplastic materials, Rev. Chem. Engng. 1, 36-69 (1983).
[4] I.C. Walton, S.H. Bittleston, The axial flow of a Bingham plastic in a narrow eccentric annulus, J. Fluid Mech. 222, 39–60 (1991).
[5] I.A. Frigaard and D.P. Ryan. Flow of a visco-plastic fluid in a channel of slowly varying width. J. Non-Newtonian Fluid Mech. 123, 67-83 (2004).
[6] S.H. Bittleston, J. Ferguson, and I.A. Frigaard, Mud removal and cement placement during primary cementing of an oil well – Laminar non-Newtonian displacements in an eccentric annular Hele-Shaw cell, J. Eng. Math. 43, 229–253 (2002).
[7] S. Pelipenko and I.A. Frigaard, Mud removal and cement placement during primary cementing of an oil well – Part 2; steady-state displacements, J. Eng. Math. 48(1), 1-26 (2004).
[8] P. Coussot, Saffman-Taylor instability in yield-stress fluids, J. Fluid Mech. 380, 363-376 (1999).
[9] J.R.A. Pearson, On suspension transport in a fracture: framework for a global model, J. Non-Newtonian Fluid Mech. 54, 503–513 (1994).
[10] P.S. Hammond, Settling and slumping in a Newtonian slurry, and implications for proppant placement during hydraulic fracturing of gas wells, Chem. Eng. Sci. 50(20), 3247-3260 (1995).
[11] S.A. Boronin, A.A. Osiptsov, Two Continua Model of Suspension Flow in a Hydraulic Fracture, Doklady Physics. 55(4), 199–202 (2010).
[12] M.R. Maxey, J.J. Riley, Equations of motion of a small rigid sphere in a non-uniform flow, Phys. Fluids. 26, 883 (1983).
[13] K.J. Scott, Hindered settling of a suspension of spheres. Critical evaluation of equations relating settling rate to mean particle diameter and suspension concentration, CSIR Report CENG 497, Chemical Engineering Research Group, Council for Scientific and Industrial Research, Pretoria, South Africa, 1984.
[14] H. Gu and E. Siebrits, On the numerical solution of hyperbolic proppant transport problems. In: Proceedings of the 10-th international conference on hyperbolic problems: theory, numerics, and applications, Osaka, Japan, September 13-17, 2004.
[15] Y. Saad, Iterative Methods for Sparse Linear Systems, 2nd Edition, SIAM 2003 - 523 pages.
[16] R.J. Leveque, High-Resolution conservative algorithms for advection in incompressible flow, SIAM J. Numer. Anal. 33(2), 627-665 (1996).
[17] N.N. Smirnov, V.F. Nikitin, A. Maximenko, M. Thiercelin, and J. C. Legros, Instability and mixing flux in frontal displacement of viscous fluids from porous media, Phys. Fluids. 17, 084102 (2005).
[18] G.M. Homsy, Viscous fingering in porous media, Ann. Rev. Fluid Mech. 19, 271-311 (1987).